Wave-equation migration Q analysis (WEMQA) from Angle-Domain Common Image Gather (ADCIG)

Yi Shen

ABSTRACT

To produce a reliable Q model, I present a new method for wave-equation migration Q analysis in angle-domain common image gathers, and develop two ways of choosing the reference images for the objective function: one using the zero angle of each angle gather and one using the zero angle of the reference angle gather. Two synthetic tests of this method demonstrate its ability to retrieve a model with Q anomalies, especially when using the zero angle of the reference angle gather. Compared with Q analysis on the stacked image, Q estimation using pre-stack gathers can obtain a higher resolution result and mitigate the side lobe problems that arise in the stacked gather.

INTRODUCTION

Shen et al. (2013) presented a new method, wave-equation migration Q analysis (WEMQA), to produce a reliable Q model. This method analyzes attenuation effects from the image space, which uses downward-continuation imaging with Q to stack out noise, focus and simplify events, and provide a direct link between the model perturbation and the image perturbation. In addition, this method uses wave-equation Q tomography to handle complex wave propagation.

However, this method is performed on the stacked image, which presents limitations. First, to remove the influence of the reflectivities on the spectra, large windows are used for the image-space spectral analysis. The use of large windows makes the spectra of the windowed reflectivities statistically identical. This generates low resolution through model building and fails when the events in the stacked image have strong horizontal variation. Second, the spectra of the image are stretched differently at different velocities, which requires spectral unstretching before spectral analysis. Third, this method stacks the pre-stack image over the offset/angle, which causes problems for the model updating. For example, the updates shown in Figure 1(a) cannot restore the shape of the true Q model in Figure 2, even when a true image perturbation is applied. The strong side lobes are the result of information loss after stacking.

I perform WEMQA on the pre-stack image, with angle-domain common image gathers, to mitigate the problem that the stacked image presents. First, if a correct velocity model is used for migration, the events in the angle gathers are flat. Therefore, this method can obtain a high resolution result without requiring large windows for the spectral analysis, and avoid the spectral differences caused by the strongly horizontal varied events. Second, no spectral correction based on the velocity is required because each depth corresponds to one velocity in the angle gathers. Third, unlike stacked images, ADCIGs preserve all the data information, which makes it possible to more correctly update the model. Figure 1(b) retrieves the shape of the true Q model in Figure 2 using a true image perturbation.

In this paper, I first present two possible objective functions for this new method. Then, I illustrate how to calculate the image perturbation. Last, I demonstrate the feasibility of this method using two 2D synthetic examples.

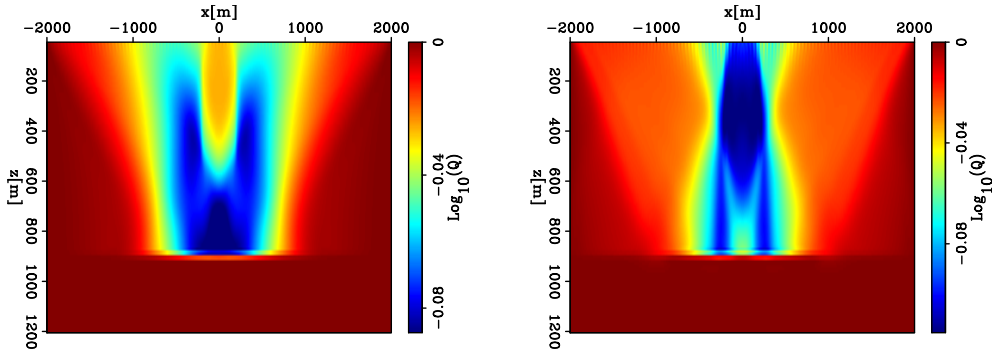

Figure 1: (a) Search direction of the true stacked image perturbation. (b) Search direction of the true pre-stack image perturbation. [**ER**]

THEORY

WEMQA from ADCIG consists of two main steps: the calculation of the image perturbation derived from the objective function, and the back projection that uses wave-equation tomography to relate the perturbed image to the model updates. Because the back projection is identical to one presented previously (Shen et al., 2013), I only describe the objective function and image perturbation.

Objective function

The goal of this method is to minimize the spectral difference of the image along the angle for each angle gather with consideration of the normal moveout (NMO) effects. The change in the spectrum can be indicated by the steepness of the slope $\rho(x, z, \gamma; Q)$, where the variable ρ is a function of spatial variable x, z, angle γ, and

the migrated Q value, and is computed by the spectral ratio method (Tonn, 1991). A larger negative slope indicates that more frequencies are attenuated. As attenuation is a frequency-dependent amplitude effect, the intercept calculated from the spectral ratio method removes frequency-independent amplitude effects such as geometric spreading, instrument response, source/receiver coupling, radiation patterns, and reflection/transmission effects. Therefore, the spectral changes are attenuation-related without the absolute scaling of the waveform. The formulation of the objective function is shown as follows:

$$J = \frac{1}{2} \sum_{x} \sum_{z} \sum_{\gamma} \|\rho\left(x, z, \gamma; Q\right)\|_2^2. \tag{1}$$

The spectral ratio method (Tonn, 1991) requires a reference spectrum to calculate the slope. I present two ways to choose the reference spectrum. The first choice is the 0° angle of each angle gather. The slope is calculated from the spectral ratio of each angle gather between a number of selected windowed events at each angle, with the windowed events at the 0° angle at the same depth. All the windows have the same size and slide down in depth. The limitations of choosing the reference spectrum in this way will be fully described in the first numerical example. The second choice is the 0° angle of a reference angle gather. This gather is carefully selected from the background image so that its 0° angle is not contaminated by attenuation. Other ways to choose the reference spectrum could be further developed, for instance, the stacked spectra over angles of each angle gather.

This method requires accurate velocity models, and its sensitivities to the velocity errors are worth investigating in the future. Fortunately, because both velocity and Q model building share the same tomography kernel, I can update these two models simultaneously.

Image perturbation estimation

The first derivative of the objective function (Equation 1) to the Q model gives the image perturbation as follows

$$\Delta I\left(x, z, h; Q\right) = \Gamma F_z^* \left[P\left(x, z, \gamma, k_z; Q\right) \mathrm{Z} \frac{2}{S\left(x, z, \gamma, k; Q\right)} \frac{1}{k} \rho\left(x, z, \gamma; Q\right) \right], \tag{2}$$

where k is the image wavenumber whose direction is perpendicular to the reflector, k_z is the vertical component of k, $S(x, z, \gamma, k; Q)$ is the spectra of the windowed events of the angle gather, Z is the operator that stretches the spectra from k to k_z, and Γ is the angle-to-offset transform. Operator F_z transforms the image $I(x, z, \gamma; Q)$ to the spatial frequency domain $P(x, z, \gamma, k_z; Q)$ (e.g., Fourier transform, continuous wavelet transform, etc.), and F_z^* is the inverse transform of F_z.

EXAMPLES

The first example to demonstrate WEMQA from ADCIG is a 2D model that is 4000 m (length) x 1200 m (depth). A horizontal reflector is at 900 m depth, and 101 sources and 401 receivers are uniformly distributed on the surface. The background medium has a constant velocity (2000 m/s) and is non-attenuating ($Q = 10000$). A rectangular Q anomaly ($Q = 20$) with the same velocity as the background medium (Figure 2), is placed above the reflector. A Ricker wavelet with 50 Hz central frequency is used as the source wavelet. I aim to invert for the Q anomaly, and I assume the background Q model and the true velocity model are known.

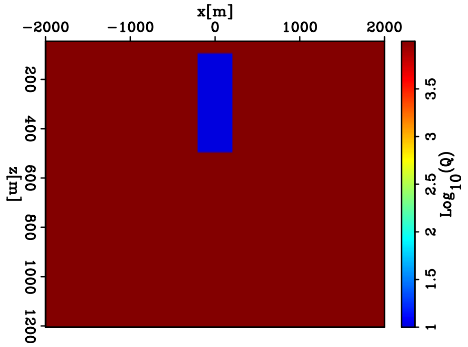

Figure 2: True Q model with a rectangular Q anomaly ($Q = 20$) and non-attenuating medium ($Q = 10000$). [**ER**]

I model the data using the true Q model (Figure 2) and use the background Q model ($Q = 10000$) as the initial model. Figures 3 and 4 are the 2D slices, from different perspectives, of the pre-stack image generated using the initial model. Figure 3 shows the power of the amplitude of a depth slice at the reflector depth ($z = 900$ m), with midpoints and angles. The weak energy forms a V shape in this figure. The wave propagates through the anomaly at the far angle where the reflection point is far from it, and at the near angle where the reflection point is under the anomaly. This interpretation of the results could be also applied to the angle gathers at different midpoints. Figure 4 shows the angle gathers at $x = 0$ m and $x = 1000$ m, respectively. The near angles are more attenuated than the far angles when the reflection occurs right below the Q anomaly. Therefore, the image in Figure 4(a) has weaker energy at the near angles than at the far angles. The opposite result is true for angle gathers at $x = 1000$ m.

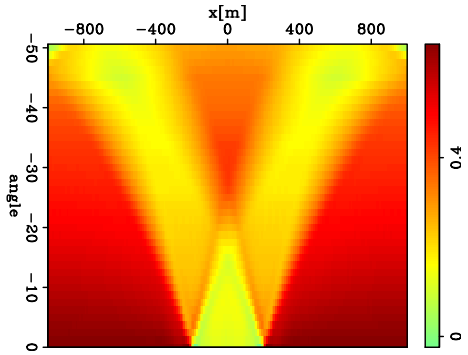

Figure 3: The power of the amplitude of a depth slice at the reflector depth ($z = 900$ m), with midpoints and angles. The weak energy forms a V shape. [**ER**]

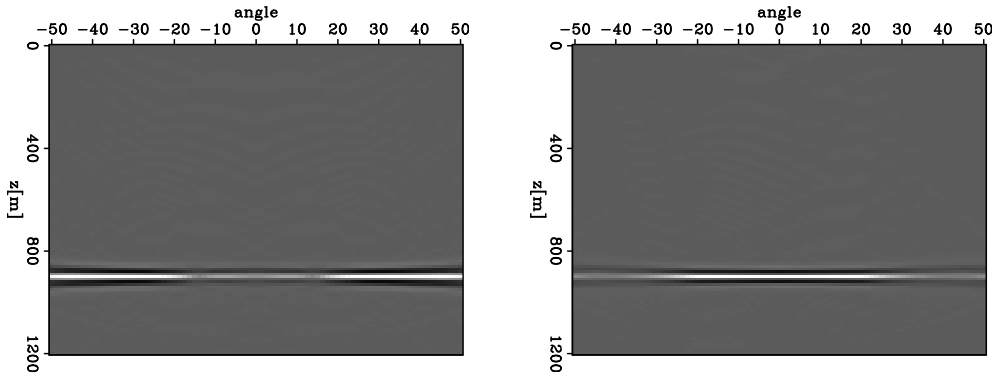

(a) (b)

Figure 4: (a) Angle gather at $x = 0$ m. The near angles are more attenuated than the far angles. (b) Angle gather at $x = 1000$ m. The far angles are more attenuated than the near angles. [**ER**]

Figures 5(a) and 5(b) show the slope value of Figure 4 by the spectral ratio method (Tonn, 1991), using the first choice of the reference spectrum (0° angle of each angle gather) described in the theory section. The positive number at the far angle in Figure 5(a) indicates that the near angle has more attenuation than the far angle; while the negative number at the far angle in Figure 5(b) demonstrates that the far angle has more attenuation than the near angle. Figures 5(c) and 5(d) are the corresponding image perturbations of Figures 5(a) and 5(b) using Equation 2; each has a different polarity. However, there are two limitations of using this method to update the model. First, because 0° angle of each angle gather is used as the reference image, there is no image perturbation and no gradient updates at the near angle, as shown in Figure 7(a). Second, less attenuation occurs at the far angle than at the near angle as the reflection point approaches to the anomaly. This condition updates the Q model a positive direction if the near angle is used as the reference. Therefore, Figure 7(b) shows unexpected positive updates of the Q value.

The second way of choosing the reference image (0° angle of the reference angle gather) overcomes the limitations of the first one by using the 0° angle at $x = 1000$ m as the reference image that is not influenced by the Q anomaly. Figures 6(a) and 6(b) accurately indicate the attenuated angle: near angles at $x = 0$ m and far angles at $x = 1000$ m. Figures 5(c) and 5(d) are the corresponding image perturbations of Figures 6(a) and 6(b) using Equation 2. Figure 7(c) shows the inversion results using this method, which retrieves the shape, location and value of the Q anomaly well.

Figures 8(a) and 8(b) show the angle gathers at $x = 0$ m migrated using the inverted Q model in Figure 7(c) and the true Q model in Figure 2, respectively. Figure 8(a), comparable to Figure 8(b), adequately compensates for the attenuated near angles in Figure 4(a). Similarly, Figure 8(c), the angle gather at $x = 1000$ m migrated with the inverted Q model, compensates for the attenuated far angles in Figure 4(b), and shows similar results as Figure 8(d), which is obtained with the true

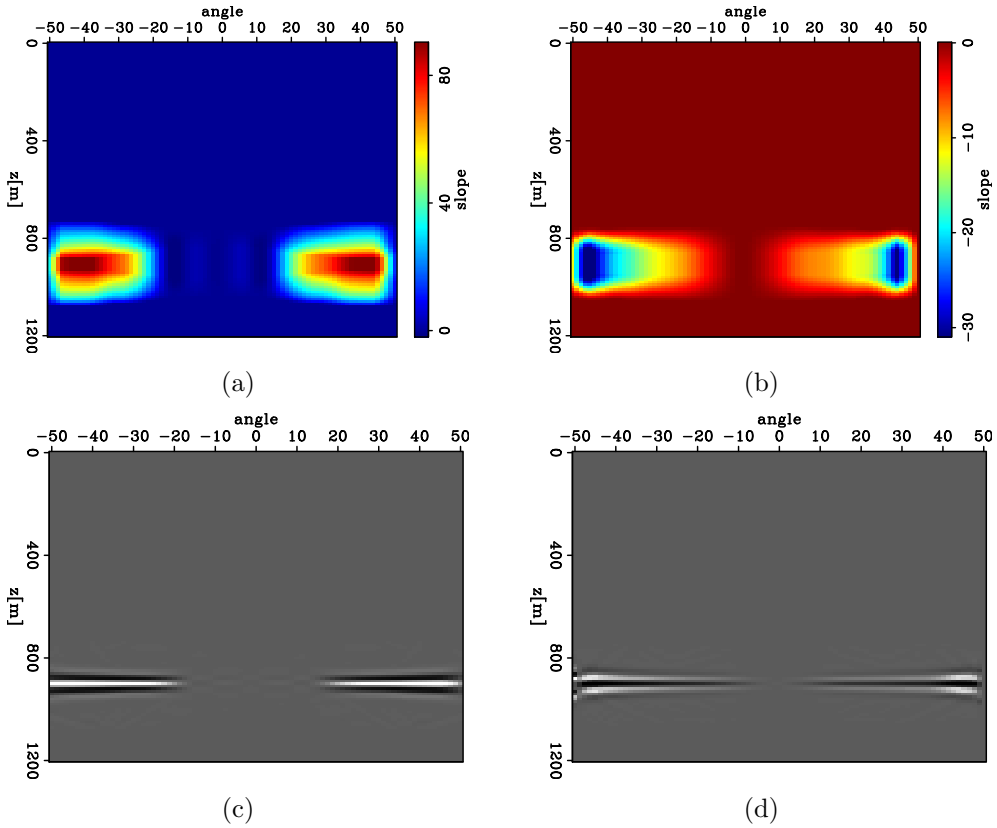

Figure 5: Using the first choice of the reference spectrum (0° angle of each angle gather), (a) the slope value of Figure 4(a), (b) the slope value of Figure 4(b), (c) the image perturbations using Figure 5(a), (d) the image perturbations using Figure 5(b). [**ER**]

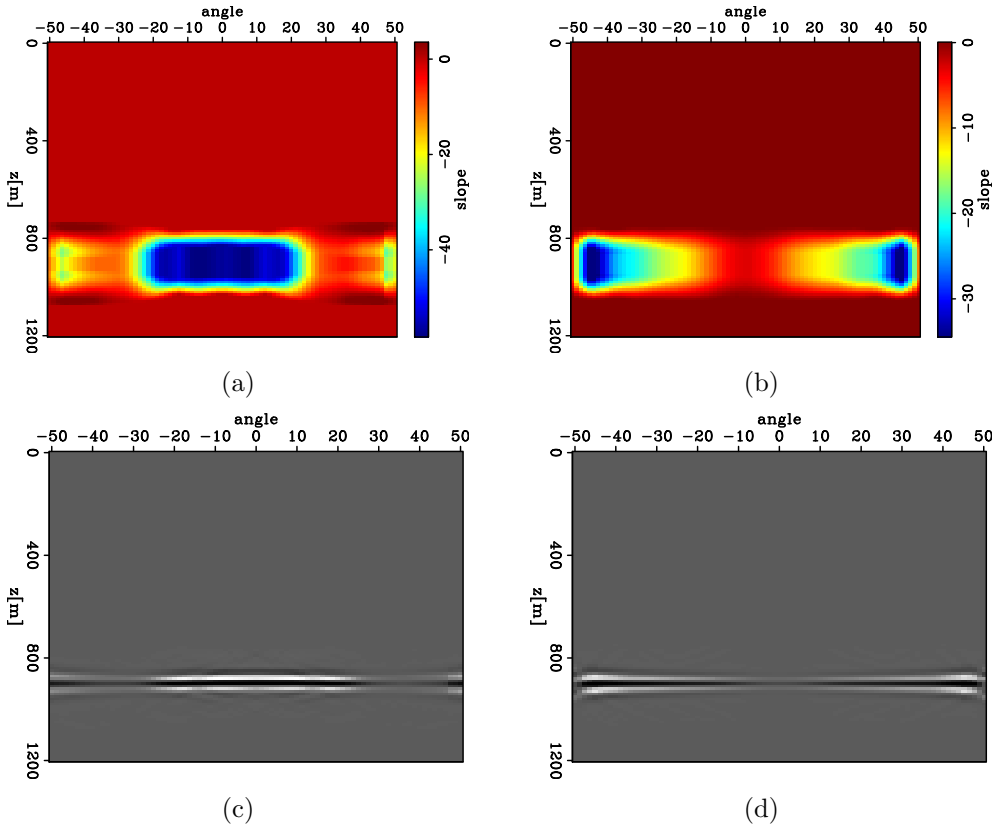

Figure 6: Using the second choice of the reference spectrum (0° angle of the reference angle gather at $x = 1000$ m), (a) the slope value of Figure 4(a), (b) the slope value of Figure 4(b), (c) the image perturbations using Figure 6(a), (d) the image perturbations using Figure 6(b). [**ER**]

Q model.

The second numerical example test employs a dataset generated by Schlumberger (Cavalca et al., 2013) using a 2D visco-acoustic version of the 2004 BP benchmark model (Billette and Brandsberg-Dahl, 2005). An attenuation model (not released) has been added by Schlumberger to the original 2004 BP models. The attenuation model is a space- and depth-variant absorption model made of several Q heterogeneities and a non-attenuative background (1/Q=0.0002). A large attenuative zone (1/Q = 0.02) is included near the left of the salt flank. In the shallow part of the model, some smaller but stronger Q heterogeneities are introduced (1/Q=[0.05,0.1]). These coincide with the gas pockets included in the original velocity model shown in Figure 9(a) and which are associated with slow-velocity anomalies. The visco-acoustic surface seismic data generated by Schlumberger used a finite-difference modeling code based on Standard Linear Solid theory. In my example, 474 shots are used with 100 m spacing, and the offsets range from -15,000 m to 15,000 m. Receivers are distributed on both sides of each shot at an increment of 25 m.

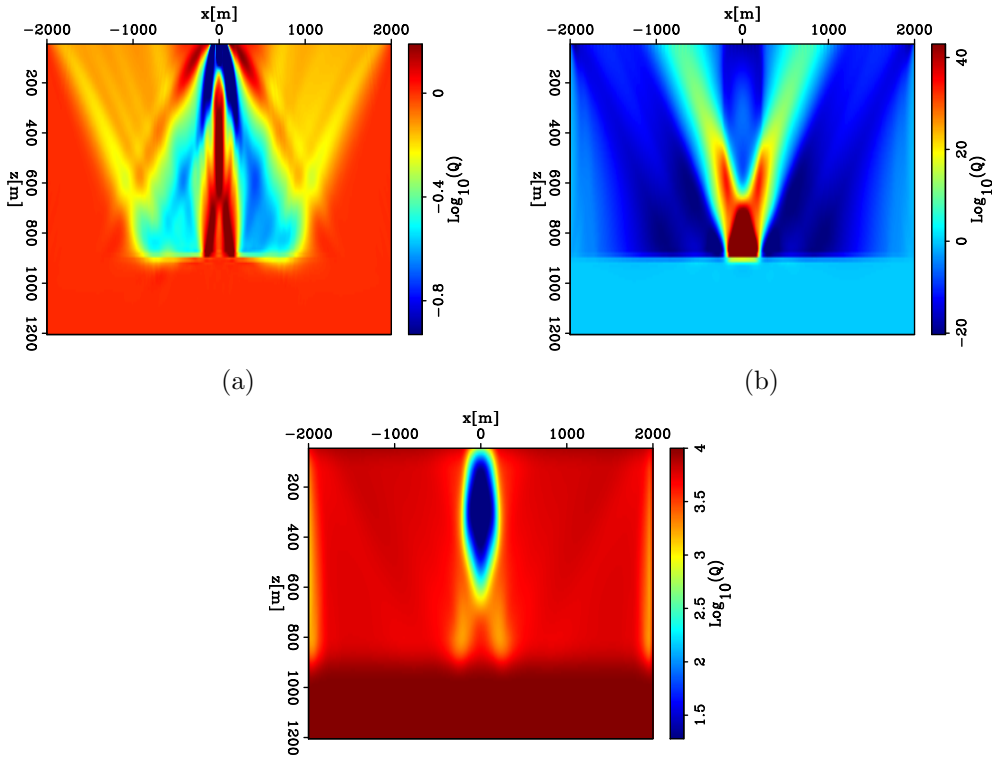

(a) (b)

(c)

Figure 7: (a) The search direction of the first iteration using the 0° angle of each gather as the reference image, with a single shot at $x = 0$ m. (b) The search direction of the first iteration using the 0° angle of each gather as the reference image, with all shots. (c) The inversion results using the 0° angle of the reference angle gather. [**ER**]

The initial model for the inversion is without attenuation. Figure 9(b) is the

migration image at zero sub- surface offset generated with the initial model. It shows the attenuated zone near the left of the salt flank and under the gas pockets. Figures 9(c) and 9(d) show the inversion results using WEMQA from the stacked image and the pre-stack image, respectively. To invert for the model from the stacked gather, we analyze the attenuation effects by calculating the slope of the logarithm of the spectral ratio between the windowed events of each trace and the events in the reference window in the same depth. Two reference traces are selected. The image to the left of the salt (x<41,025 m) is compared with the reference trace at x=20,450 m; while the image to the right of the salt (x>41,025 m) is compared with the reference trace at x=42,000 m. To analyze the pre-stack gather, I choose the 0° angles at $x = 25000$ m as the reference.

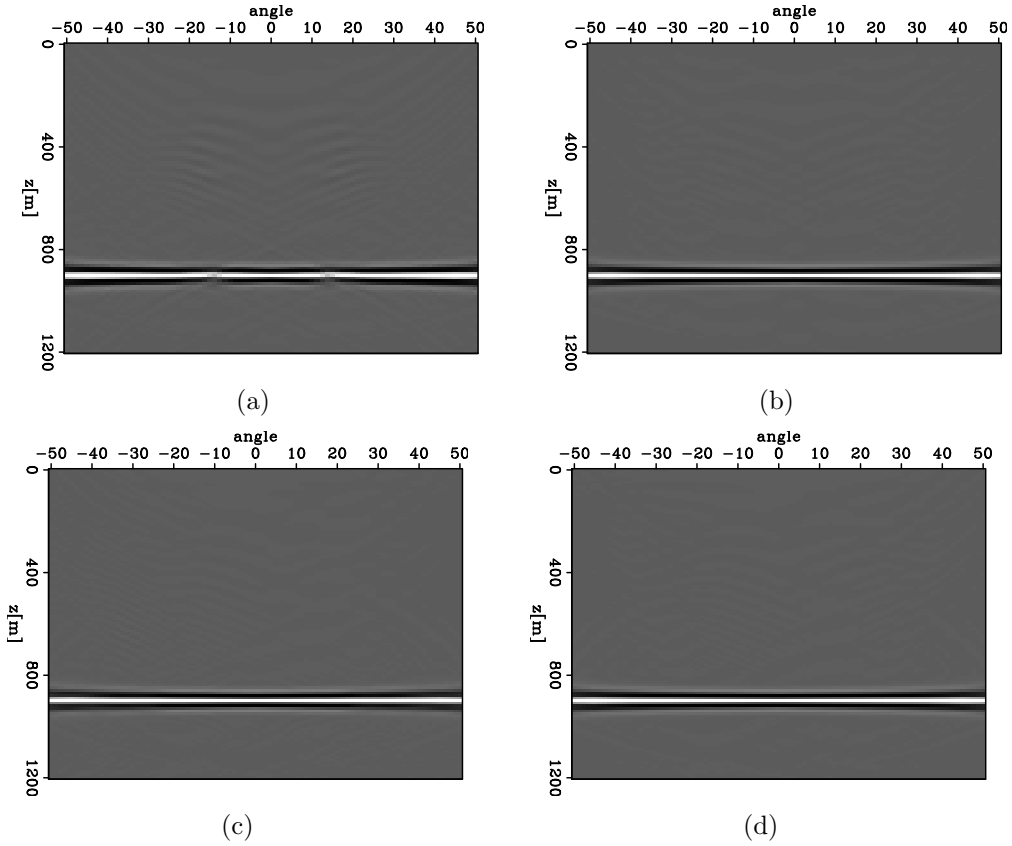

Figure 8: (a) Angle gather at $x = 0$ m migrated using the inverted Q model in Figure 7(c). (b) Angle gather at $x = 0$ m migrated using the true Q model in Figure 2. (c) Angle gather at $x = 1000$ m migrated using the inverted Q model in Figure 7(c). (d) Angle gather at $x = 1000$ m migrated using the true Q model in Figure 2. [**ER**]

Figure 9(c) shows that the locations of the gas pockets and the attenuating zone beside the salt are well retrieved. However, the side lobes of the inverted gas pockets are very strong. With the help of the pre-stack gather, the inverted model in Figure 9(d) has slightly better resolution, and the side lobe problem of the gas pockets is mitigated. However, both results have low resolution. One main reason for the poor

resolution is that tomography updates the low wavenumber components. Another explanation for the low vertical resolution is that with a reasonable depth range, the attenuation below the gas pockets is stronger than that within the gas. The first few iterations focus the updates below the gas, but the update will gradually move up to the gas pockets as iteration continues. In addition, the attenuating zone beside the salt is not as well retrieved as the gas pockets, especially for the pre-stack method shown in Figure 9(d). The steepness of the salt flank makes the one-way wave propagation fail in imaging, and it introduces artifacts and errors in the spectral analysis. Therefore, I will use two-way migration with Q (Zhu et al., 2014) for a better image of the salt.

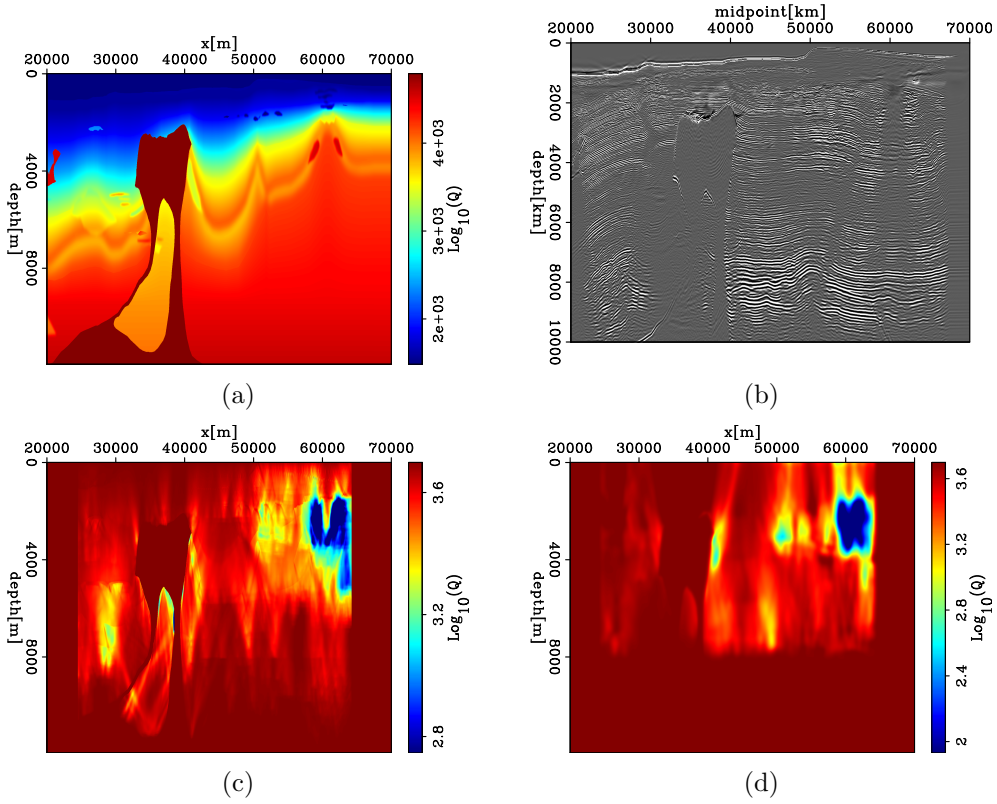

Figure 9: (a) 2004 BP benchmark velocity model (Billette and Brandsberg-Dahl, 2005). (b) The migration image at zero sub-surface offset generated with the initial model. (c) The inversion results using WEMQA from the stacked image. (d) The inversion results using WEMQA from the pre-stack image. [**CR**]

CONCLUSION

This paper presented a new method that uses wave-equation migration Q analysis from angle-domain common image gathers (ADCIG) to produce a reliable Q model. Two ways of choosing the reference images for the objective function were developed: 0° angle of each angle gather and 0° angle of the reference angle gather. Two 2D

synthetic tests of this method demonstrated its ability to retrieve the model with Q anomalies. Also, performing both ways of choosing of the reference images in the first example shows the advantages of using 0° angle of the reference angle gather. Compared with Q analysis from the stacked image in the second example, Q estimation using pre-stack gathers can obtain a higher resolution result and can mitigate the side lobes problem that occurs in the stacked image.

ACKNOWLEDGMENTS

The author thanks Biondo Biondi, Robert Clapp and Dave Nichols of Stanford for their advice and suggestions, and also thanks Schlumberger and BP for providing the 2D synthetic dataset.

REFERENCES

Billette, F. and S. Brandsberg-Dahl, 2005, The 2004 BP velocity benchmark: 67th Conference and Exhibition, EAGE, Extended Abstracts.

Cavalca, M., R. P. Fletcher, and M. Riedel, 2013, Q-compensation in complex media ray-based and wavefield extrapolation approaches: 83rd Annual International Meeting, SEG, Expanded Abstracts.

Shen, Y., B. Biondi, R. Clapp, and D. Nichols, 2013, Wave-equation migration Q analysis (WEMQA): EAGE Workshop on Seismic Attenuation Extended Abstract 2013.

Tonn, R., 1991, The determination of seismic quality factor Q from VSP data: A comparison of different computational techniques: Geophysical Prospecting, **45**, 87–109.

Zhu, T., J. Harris, and B. Biondi, 2014, Q-compensated reverse-time migration: GEOPHYSICS, **79**, S77–S87.